# Photonic-crystal scintillators: molding the flow of light to enhance x-ray and gamma-ray detection

**Yaniv Kurman[1], Avner Shultzman[1], Ohad Segal[1] Adi Pick[2], and Ido Kaminer[1]**

[1]Department of Electrical Engineering, Technion, Israel Institute of Technology, 32000 Haifa, Israel

[2]Chemistry Department, Weizmann Institute, 7610001 Rehovot, Israel

## Supplementary Materials

## Contents

**1. Statistical analysis of a conventional scintillation structure** **3**

**2. Statistical analysis of a nanophotonic scintillation structure** **5**

**3. Extraction of the spectral distribution $Y(\omega)$ and emission rate $\Gamma_0(\omega)$, from the given spectra $S(\omega)$ and decay time $\tau_d$** **8**

**4. Deriving the Purcell factor in a general layered media** **10**

**5. Deriving the Purcell factor for an infinite photonic crystal** **15**

**6. The photonic structure's partial emission properties** **17**

In this Supplementary Material, we provide the complete formalism that demonstrates how the Purcell effect can improve the scintillation process. We develop the formalism for the scintillator's effective emission rate and efficiency, including the outcoupling of the emitted scintillation photon from the structure. In the first part (sections 1-3), we focus on the statistical model and generalize it to an arbitrary geometrical configuration. In the second part (sections 4-5), we show how to calculate the Purcell enhancement for a one-dimensional (1D) Photonic crystal (PhC) structure, whether it is infinite or finite. Then, in section S6, we present different parameters for describing the advantages of the photonic structure, which can be used to define figures-of-merits for different applications.

## S.1 Statistical analysis of a conventional scintillation structure

In this section, we introduce the statistical model of the scintillation process for a bulk scintillation medium. There are three effective parameters that describe the scintillation process: the rise time $\tau_r$, the bulk decay time $\tau_{d,0}$, and the number of extracted photons for a given radiation energy (light yield) $n_0$. The rise time represents the time it takes from the radiation arrival to the beginning of scintillation. The rise time includes the conversion of the radiation into a photoelectric electron, the production of electron-hole pairs by this electron, and the thermalization of the pairs until reaching recombination in the luminescence centers. Thus, the rise time is usually in the order of tens of ps (60 ps for LYSO:Ce). The improvement of the rise time could also be potentially achieved with nanophotonics, but it is not the focus of this paper. The decay time describes the typical time in which a photon is spontaneously emitted from the luminescence center. The decay time is usually in the order of tens of ns or more in inorganic scintillators (40 ns for LYSO:Ce), and it can be shorten by changing the optical medium inside the scintillator, as we show here.

Overall, in order to include both the rise and decay times as independent processes, the scintillation-photon emission probability density function $f(t)$ is calculated as a convolution between two exponential distributions,

$$f(t) = \left[\frac{e^{-\frac{t}{\tau_r}}\Theta(t)}{\tau_r}\right] * \left[\frac{e^{-\frac{t}{\tau_{d,0}}}\Theta(t)}{\tau_{d,0}}\right] = \int_{\infty}^{\infty} \frac{e^{-\frac{t'}{\tau_r}}\Theta(t')}{\tau_r} \frac{e^{-\frac{(t-t')}{\tau_{d,0}}}\Theta(t-t')}{\tau_{d,0}} dt' = \frac{e^{-\frac{t}{\tau_{d,0}}} - e^{-\frac{t}{\tau_r}}}{\tau_{d,0} - \tau_r}\Theta(t), \quad \text{(S1)}$$

where $\Theta(t)$ is the step function starting at the arrival of the energetic radiation. By integrating Eq. (S1) over time, we get the cumulative distribution function (CDF) to find the probability that a photon arrived at the detector until time $t$,

$$F(t)=\int_0^t f(t')dt'=\left[1-\frac{\tau_{d,0}e^{-\frac{t}{\tau_d}}-\tau_r e^{-\frac{t}{\tau_r}}}{\tau_{d,0}-\tau_r}\right]\Theta(t). \quad \text{(S2)}$$

This statistical analysis also enables to estimate what is the arrival time correlation of the first photon between two detectors, which is important in applications such as time-of-flight PET scan. Using a Taylor expantion for small times $t$ in Eq. (S2), the CDF goes like time squared, $F(t)=\frac{t^2}{2\tau_r(\tau_{d,0}-\tau_r)}\cong\frac{t^2}{2\tau_r\tau_{d,0}}$. Now, since all emitted photons are independent, the expectation value of the number of photons that reach the detector until time $t$ is $N_t=n_0\frac{t^2}{2\tau_r\tau_{d,0}}$. Moreover, the probability that $k$ photons will arrive until time $t$ has a poissonian distributed [1], $P_k(t)=\frac{(N_t)^k e^{-N_t}}{(k)!}$. Consequently, the probability that the $k^{\text{th}}$ photon is arriving to the detector exactly between $t$ and $t+dt$ is

$$W_k(t)=P_{k-1}(t)\frac{d(N_t)}{dt}=\frac{(N_t)^{k-1}e^{-N_t}}{(k-1)!}\cdot\frac{d(N_t)}{dt}\cong\frac{n_0 t}{\tau_r\tau_d}\frac{\left(\frac{n_0t^2}{2\tau_r\tau_{d,0}}\right)^{k-1}e^{-\frac{t^2}{2\tau_r\tau_{d,0}}{n}}}{(k-1)!}\Theta(t). \quad \text{(S3)}$$

Finally, the resolution in detection of the $k$'th photon arrise from the full-width-half-maximum (FWHM) of the cross-correlation function, $R_k(t)=\int_{-\infty}^{\infty}W_k(\tau)W_k(t+\tau)d\tau$, between the two opposite-directional detectors with similar statistics. Specifically, the FWHM formula for the first photon is then

$$\text{FWHM}(k=1)=4\sqrt{\ln(2)}\,\text{var}\big(W_{k=1}(\tau)\big)=4\sqrt{\ln(2)}\sqrt{\frac{4-\pi}{2}\frac{\tau_r\tau_{d,0}}{n}}. \quad \text{(S4)}$$

The analysis shows that this FWHM, called also the coincidence time resolution (CTR), is proportional to $\sqrt{\frac{\tau_r\tau_{d,0}}{n}}$. In Fig. 1c in the main text, we show in purple the cross-correlation function $R_{k=1}(t)$ for a LYSO:Ce scintillator, and calculate its CTR according to Eq. (S4).

## S.2 Statistical analysis of a nanophotonic scintillation structure

We now generalize the statistical analysis by considering the dependence of the decay time on the optical environment (the rise time remians the same). The Purcell factor $F_P$ alters the bare emission rate $\Gamma_0(\omega)$ (that in conventional scintillators depends only on the emission frequency $\omega$) into an effective emission rate,

$$\Gamma_{\text{eff}}(z,\omega,\theta) = \sum_{\sigma} \Gamma_0^{\sigma}(\omega) F_{\text{P}}^{\sigma}(z,\omega,\theta) T^{\sigma}(z,\omega,\theta), \tag{S5}$$

which depends on the emission direction $\theta$ (relative to the $z$ axis), the emission location in space $z$ (in 1D), and $\sigma \in \{\text{TE}, \text{TM}\}$ the light's polarization. In addition, we introduced the transmission coefficient ,$T^{\sigma}(z,\theta,\omega)$, to count only the photons that were able to escape the scintillator. To take into account the spectral distribution of the emission, we next multiply $\Gamma_{\text{eff}}(z,\omega,\theta)$ by the normalized distribution function $Y(\omega)$ of the emitting material, defined so that $\int Y(\omega)d\omega = 1$. We determine $Y(\omega)$ through the emission spectrum of a bulk medium (see section S.3); it can be understood as the amount of luminescence with emission frequency $\omega$ compared to the total luminescence. Considering all the above, the probability density function (Eq. (S1)) takes the form

$$f(t) = \left(\frac{e^{-\frac{t}{\tau_r}}\Theta(t)}{\tau_r}\right) * \left[\int d\omega Y(\omega) \int_0^{\frac{\pi}{2}} \sin(\theta)\, d\theta \int_0^{L} dz G(z)\, \Gamma_{\text{eff}}(z,\omega,\theta) e^{-\Gamma_{\text{eff}}(z,\omega,\theta)t}\Theta(t)\right]$$

$$= \int d\omega Y(\omega) \int_0^{\frac{\pi}{2}} \sin(\theta)\, d\theta \int_0^{L} G(z) dz \frac{e^{-\Gamma_{\text{eff}}(z,\omega,\theta)t} - e^{-\frac{t}{\tau_r}}}{\Gamma_{\text{eff}}^{-1}(z,\omega,\theta) - \tau_r}\Theta(t), \tag{S6}$$

where $L$ is the length of the whole structure, and $G(z)$ is the spatial distribution of emitters which we take as uniform inside the scintillation materiall and zero in the dielectric, and normalize so that $\int_0^L dz G(z) = 1$.

With the same step as in section S.1, the CDF for the probability that a photon arrived to the detector until a time $t$ is

$$F(t) = \int d\omega Y(\omega) \int_0^{\frac{\pi}{2}} \sin(\theta)\, d\theta \int_0^L G(z) dz \left[ 1 - \frac{\frac{e^{-\Gamma_{\text{eff}}(z,\omega,\theta)t}}{\Gamma_{\text{eff}}(z,\omega,\theta)} - \tau_r e^{-\frac{t}{\tau_r}}}{\Gamma_{\text{eff}}^{-1}(z,\omega,\theta) - \tau_r} \right]$$

$$\cong \frac{t^2}{2\tau_r} \int d\omega Y(\omega) \int_0^L G(z) dz \int_0^{\frac{\pi}{2}} \sin(\theta)\, d\theta\, \Gamma_{\text{eff}}(z,\omega,\theta) \equiv \frac{\Gamma_{\text{eff}}}{2\tau_r} t^2. \quad \text{(S7)}$$

The approximation in Eq. (S7) is correct only at times where $t \ll \tau_r, \Gamma_{\text{eff}}^{-1}(z,\omega,\theta)$. From Eq. (S7), we can connect the decay rate of the structure, $\tau_d$, to the average effective emission rate (as in Eq. (1) in the main text),

$$\Gamma_{\text{eff}} = \frac{1}{\tau_d} = \int d\omega Y(\omega) \int_0^{\frac{\pi}{2}} \sin(\theta)\, d\theta \int_0^L G(z) dz \sum_\sigma \Gamma_0^\sigma(\omega) F_{\text{P}}^\sigma(z,\omega,\theta) T^\sigma(z,\omega,\theta)\,. \quad \text{(S8)}$$

Another significant effect that the Purcell effect has on the scintillation properties is increasing the total number of detectable photons. Defining the total number of emitted photons inside the structure, $N_0$, to account for the number of electron-hole pairs that recombine radiativly, we find the number of detectable photons $n$ is

$$n = N_0 \frac{\int d\omega Y(\omega) \int_0^{\frac{\pi}{2}} \sin(\theta)\, d\theta \int_0^L G(z) dz \sum_\sigma \Gamma_0^\sigma(\omega) F_{\text{P}}^\sigma(z,\omega,\theta) T^\sigma(z,\omega,\theta)}{\int d\omega Y(\omega) \int_0^{\frac{\pi}{2}} \sin(\theta)\, d\theta \int_0^L G(z) dz \sum_\sigma \Gamma_0^\sigma(\omega) F_{\text{P}}^\sigma(z,\omega,\theta)}.$$

In a standard scintilator, as described in section S.1, the emission rate is isotropic so that the number of emitted photons is $n_0 = N_0 \frac{\int d\omega Y(\omega) \int_0^{\frac{\pi}{2}} \sin(\theta) d\theta \sum_\sigma \Gamma_0^\sigma(\omega) T_0^\sigma(\omega,\theta)}{\int d\omega Y(\omega) \sum_\sigma \Gamma_0^\sigma(\omega)}$, where $T_0^\sigma(\omega,\theta)$ is the transmission coefficient to outcouple light from the bulk. Now, we can define also the efficiency $\eta$ as enhancement of the number of detectable photons (as in Eq. (2) in the main text),

$$\eta = \frac{n}{n_0} = \frac{\frac{\int d\omega Y(\omega) \int_0^{\frac{\pi}{2}} \sin(\theta)\, d\theta \int_0^L G(z) dz \sum_\sigma \Gamma_0^\sigma(\omega) F_{\mathrm{P}}^\sigma(z,\omega,\theta) T^\sigma(z,\omega,\theta)}{\int d\omega Y(\omega) \int_0^{\frac{\pi}{2}} \sin(\theta)\, d\theta \int_0^L G(z) dz \sum_\sigma \Gamma_0^\sigma(\omega) F_{\mathrm{P}}^\sigma(z,\omega,\theta)}}{\frac{\int d\omega Y(\omega) \int_0^{\frac{\pi}{2}} \sin(\theta)\, d\theta \sum_\sigma \Gamma_0^\sigma(\omega) \sqrt{\varepsilon(\omega)} T_0^\sigma(z,\omega,\theta)}{\int d\omega Y(\omega) \sum_\sigma \Gamma_0^\sigma(\omega) \sqrt{\varepsilon(\omega)}}}, \qquad \text{(S9)}$$

where $\sqrt{\varepsilon(\omega)}$ is the scintillator's refractive index (described through its permittivity $\varepsilon$), which equals to the bulk's Purcell factor [2]. Using Eq. (S7) and (S9), we find that $\eta F(t)$ is the number of photons that reach the detector before time $t$, normalized by $n_0$, shown in Fig. 1b in the main text.

As a result of changing the effective emission rate and the efficiency, the CTR can also be improved. Since the emitted photons are still independent, the expectation number of photons that reach the detector until time $t$ for short times, is now $N_t = n\frac{\Gamma_{\mathrm{eff}}}{2\tau_r}t^2$, which is the same expectation value as in Section S.1 except of using $\Gamma_{\mathrm{eff}}$ instead of $\frac{1}{\tau_d}$. From here, the rest of the analysis is similar to Section S.1 for the probability for the k'th photon detection, as in Eq. (S3), is $W_k(t) \cong 2n\frac{\Gamma_{\mathrm{eff}}}{2\tau_r} t \frac{\left(n\frac{\Gamma_{\mathrm{eff}}}{2\tau_r}t^2\right)^{k-1} e^{-n\frac{\Gamma_{\mathrm{eff}}}{2\tau_r}t^2}}{(k-1)!}\Theta(t)$, and the CTR is

$$\mathrm{FWHM}(k=1) = 4\sqrt{\ln(2)}\,\mathrm{var}(W_{k=1}) = 4\sqrt{\ln(2)}\sqrt{\frac{4-\pi}{2}\frac{\tau_r}{\eta n_0 \Gamma_{\mathrm{eff}}}}.$$

Overall, we see that the CTR is now improved by both the effective emission rate and by the efficiency, with a total enhancement factor of $\sqrt{\frac{1}{\eta\tau_{d,0}\Gamma_{\mathrm{eff}}}}$. According to this result, we will optimize our structure to maximize the parameter $\eta\tau_{d,0}\Gamma_{\mathrm{eff}}$. In Fig. 1c in the main text we show the CTR of a PhC structure compared to the CTR of a bulk scintillator.

## S.3 Extraction of the spectral distribution $Y(\omega)$ and emission rate $\Gamma_0(\omega)$, from the given spectra $S(\omega)$ and decay time $\tau_d$

When changing the optical structure, we were able to manipulate the emission rate enhancement per frequency and angle for each location in space. However, the parameters that are known from the literature are the decay time $\tau_{d,0}$ and the emission spectra $S(\omega)$, rather than $\Gamma_0(\omega)$ and $Y(\omega)$. In this section, we show how we convert the parameters from the literature to derive the required quantities.

According to Fermi's golden rule, the emission rate in homogeneous media is the multiplication of the bare emission rate and the material's refractive index [2], $\sqrt{\varepsilon(\omega)}$, so that:

$$\Gamma_{\mathrm{h}}(\omega) = \Gamma_0(\omega)\sqrt{\varepsilon(\omega)} = \frac{4\alpha\omega^3|\boldsymbol{\mu}(\omega)|^2}{3c^2}\sqrt{\varepsilon(\omega)}\,, \tag{S10}$$

where $c$ is the vacuum speed of light, and $\alpha$ is the fine-structure constant. In addition, $\boldsymbol{\mu}(\omega)$ is the intrinsic dipole moment of the luminescence center, which does not change when altering the electromagnetic environment under the conditions of this paper. We find the connection between the decay time $\tau_{d,0}$, $\Gamma_0(\omega)$, and $Y(\omega)$, by comparing Eq. (S1) and (S6) in a homogeneous medium:

$$\frac{e^{-\frac{t}{\tau_d}} - e^{-\frac{t}{\tau_r}}}{\tau_d - \tau_r} = \int \mathrm{d}\omega Y(\omega) \int_0^{\frac{\pi}{2}} \sin(\theta)\,\mathrm{d}\theta \, \frac{e^{-\sum_\sigma \Gamma_{\mathrm{h}}^\sigma(\omega)T^\sigma(\omega,\theta)t} - e^{-\frac{t}{\tau_r}}}{\left(\sum_\sigma \Gamma_{\mathrm{h}}^\sigma(\omega)T^\sigma(\omega,\theta)\right)^{-1} - \tau_r}\,.$$

Thus, similar to section S.2, we can find the connection:

$$\frac{1}{\tau_{d,0}} = \int \mathrm{d}\omega Y(\omega) \int_0^{\frac{\pi}{2}} \sin(\theta)\,\mathrm{d}\theta \sum_\sigma T^\sigma(\omega,\theta)\Gamma_{\mathrm{h}}^\sigma(\omega)\,. \tag{S11}$$

This connection enables to find $\Gamma_{\mathrm{h}}(\omega)$ and the dipole moment $|\boldsymbol{\mu}(\omega)|$, provided we have $Y(\omega)$ and taking $\Gamma_{\mathrm{h}}^{\mathrm{TE}}(\omega) = \Gamma_{\mathrm{h}}^{\mathrm{TM}}(\omega) = \Gamma_{\mathrm{h}}(\omega)/2$ .

Fortunately, we can find $Y(\omega)$ by taking the emission spectrum $S(\omega)$ of the material from the literature. The emission spectrum in some sources relate to the number of photons per second that reach the detector per frequency so that,

$$S(\omega) = \beta Y(\omega)\Gamma_{\mathrm{h}}(\omega)T_0(\omega)\,,$$

where $\beta = \frac{\Gamma_{\mathrm{h}}}{\Gamma_{\mathrm{h}}+\Gamma_{\mathrm{nr}}}$ is the ratio between the radiative and overall relaxation rates (including non-radiative decay), and $T_0(\omega) = \int d\theta \sin(\theta)\,(T_0^{TM}(\theta,\omega) + T_0^{TE}(\theta,\omega))$ is the transmission coefficient for outcoupling the emission from the scintillator into free-space. Assuming a constant dipole moment for each frequency and $\beta = 1$, we substitute Eq. (S10) to find the spectral distribution,

$$Y(\omega) = \frac{\dfrac{S(\omega)}{\omega^3\sqrt{\varepsilon(\omega)}T_0(\omega)}}{\int d\omega\left[\dfrac{S(\omega)}{\omega^3\sqrt{\varepsilon(\omega)}T_0(\omega)}\right]}\,, \tag{S12}$$

normalized so that $\int \mathrm{d}\omega Y(\omega) = 1$. Substituting into Eq. (S11) we can find the dipole moment and consequently also the emission rate for each frequency,

$$|\boldsymbol{\mu}|^2 \cong \frac{3\pi\epsilon_0\hbar c^3}{\tau_d \int \mathrm{d}\omega Y(\omega)\omega^3\sqrt{\varepsilon(\omega)}T_0(\omega)}. \tag{S13}$$

When substituting the dipole moment into Eq. (S10), the emission rate $\Gamma_0(\omega)$ is found.

## S.4 Deriving the Purcell factor in a general layered media

In this section, we review how to calculate the emission rate and the Purcell factor in any layered medium. In a general structure, the emission rate of a local dipole $\boldsymbol{\mu} = e\langle \mathrm{i}|\boldsymbol{r}|\mathrm{f}\rangle$ where $|\mathrm{i}\rangle$, $|\mathrm{f}\rangle$ are the initial and final state, is calculated through [2]:

$$\Gamma_{\text{dipole approx.}} = \frac{2\omega}{\epsilon_0 \hbar \mathrm{c}^2} \mathrm{Im}\left[\boldsymbol{G}_{\hat{\boldsymbol{\mu}}\hat{\boldsymbol{\mu}}}(\boldsymbol{r_0}, \boldsymbol{r_0}; \omega)\right] |\boldsymbol{\mu}|^2 , \tag{S14}$$

where $\boldsymbol{r_0}$ is the location of the dipole, $\epsilon_0$ is the vacuum permittivity, and $\hbar$ is the reduced Planck's constant. In addition, $\boldsymbol{G}_{ij}(\boldsymbol{r}, \boldsymbol{r}'; \omega)$ is the dyadic Green's function which describes the $i^{th}$component of the electric field in location $\boldsymbol{r}$ as a result of a dipole excitation in $\boldsymbol{r}'$ oriented along $j$. This Green's function captures the electromagnetic response of the entire structure (including its optical environment). In our structure, we can assume the dipole approximation for the scintillation emitters (luminescence centers), so that the emission is captured by $\mathrm{Im}\left[\boldsymbol{G}_{\hat{\boldsymbol{\mu}}\hat{\boldsymbol{\mu}}}(\boldsymbol{r_0}, \boldsymbol{r_0}; \omega)\right]$, which is proportional to the local density of photonic states (LDOS) of the dipole emission at point $\boldsymbol{r_0}$ and orientation $\hat{\boldsymbol{\mu}}$. Thus in this work, the emission rate, the Purcell factor, and the LDOS are all proportional to one another and are manipulated through our photonic design.

The structures that we analyze are finite or infinite 1D photonic crystals which are specific cases of a multi-layer structure. In such structure, the reflection from each one of the layers causes a constructive or destructive interference for each frequency and propagation angle so that the LDOS varies strongly between different photonic modes. Because of the translational symmetry in the system, the dyadic Green's function is expressed by a mode expansion according to the in-plane momentum $\boldsymbol{q} = (q_x, q_y)$ [3, 4]:

$$\overleftrightarrow{\boldsymbol{G}}(\boldsymbol{r},\boldsymbol{r},\omega)=\frac{i}{8\pi^2}\int d\boldsymbol{q}\,\frac{1}{\varepsilon_m q^2 k_{m,z}}\left[G_{\parallel}^{TM}(q,z)\hat{\boldsymbol{q}}\hat{\boldsymbol{q}}+G_{\perp}^{TM}(q,z)\hat{\boldsymbol{z}}\hat{\boldsymbol{z}}+\hat{\boldsymbol{q}}\hat{\boldsymbol{q}}G_{\parallel}^{TE}(\boldsymbol{q},z)\right]. \quad \text{(S15)}$$

$k_{m,z}=\sqrt{\varepsilon_m\omega^2/c^2-q^2}$ is the wave vector in the $\hat{z}$ direction with $\varepsilon_m$ as the permittivity of the material in the $m^{\text{th}}$ layer. In Eq. (S15), $G_{\perp,\parallel}^{\sigma}$ represents the spectral response for the polarizations $\sigma$ and dipole excitation in the perpendicular ($\perp$) or parallel ($\parallel$) directions, calculated through

$$G_{\parallel}^{\sigma}(z,\omega,q)=\frac{\left[e^{-ik_{m,z}z}+e^{ik_{m,z}(z+2d_m)}\tilde{R}_{m,m+1}^{\sigma}\right]\left[e^{ik_{m,z}z}+e^{-ik_{m,z}(z+2d_{m-1})}\tilde{R}_{m,m-1}^{\sigma}\right]}{1-\tilde{R}_{m,m+1}^{\sigma}\tilde{R}_{m,m-1}^{\sigma}e^{2ik_{1,z}(d_m-d_{m-1})}}, \quad \text{(S16a)}$$

$$G_{\perp}^{TM}(z,\omega,q)=\frac{\left[e^{-ik_{m,z}z}-e^{ik_{m,z}(z+2d_m)}\tilde{R}_{m,m+1}^{TM}\right]\left[e^{ik_{m,z}z}-e^{-ik_{m,z}(z+2d_{m-1})}\tilde{R}_{m,m-1}^{TM}\right]}{1-\tilde{R}_{m,m+1}^{TM}\tilde{R}_{m,m-1}^{TM}e^{2ik_{1,z}(d_m-d_{m-1})}}, \quad \text{(S16b)}$$

where $-d_m$ is the location of the interface between the $m^{\text{th}}$ and the $(m+1)^{\text{th}}$ layers. In this configuration, $z=0$ is the location of the last interface (i.e., the whole structure is in $z<0$), and the outcoupled emitted light is propagating towards the positive z axis. $\tilde{R}_{m,m+1}^{\sigma}$ are the global reflection coefficients from the whole optical structure at each interface, calculated in a recursive manner according to the reflection from the next interface [3],

$$\tilde{R}_{m,m+1}^{\sigma}=\frac{r_{m,m+1}^{\sigma}+\tilde{R}_{m+1,m+2}^{\sigma}e^{2ik_{m+1,z}(d_{m+1}-d_m)}}{1+r_{m,m+1}^{\sigma}\tilde{R}_{m+1,m+2}^{\sigma}e^{2ik_{m+1,z}(d_{m+1}-d_m)}}, \quad \text{(S17)}$$

where $r_{12}^{TE}=\frac{k_{1z}-k_{2z}}{k_{1z}+k_{2z}}$, $r_{12}^{TM}=\frac{\epsilon_1 k_{2z}-\epsilon_2 k_{1z}}{\epsilon_2 k_{1z}+\epsilon_1 k_{2z}}$ are the Fresnel coefficients. Note that the last interface of the structure satisfies $\tilde{R}_{m+1,m+2}^{\sigma}=0$, so that $\tilde{R}_{m,m+1}^{\sigma}=r_{m,m+1}^{\sigma}$ (the conventional Fresnel coefficient). Eq. (S17) is in fact equivalent to the common transfer matrix equations so that with any given boundary conditions, the effective reflection coefficient from each interface can be derived. Moreover, since these coefficients relate to the reflection from *the entire structure*, the transmission into the external material for each layer and polarization is calculated by

$$T_m^{\sigma}(\omega, q) = 1 - \left|\tilde{R}_{m,m-1}^{\sigma}(\omega, q)\right|^2.$$

In Fig. S1, we present an example of the spectral response near the edge of a photonic crystal. We see the typical differences between $G_{\parallel}(z, \lambda = \frac{2\pi c}{\omega}, \theta = 0)$ and $G_{\perp}^{TM}(z, \lambda = \frac{2\pi c}{\omega}, \theta = 0)$, with one getting a maximal value at the center of the layer at the same positions for which the other gets a minimal value. This plot shows that for our specific structure and wavelengths of emission, a dipole oriented in the x-y plane would maximize its perpendicular emission when located at the edges of the layer.

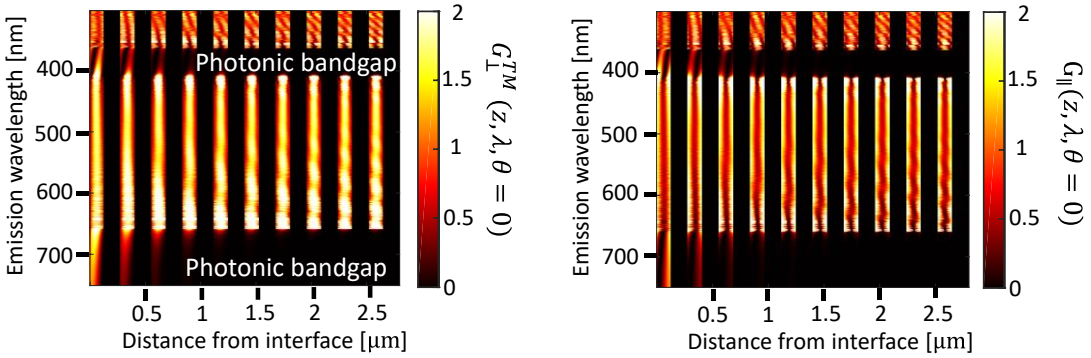


**Figure S1: The typical spectral response near the edge of a Photonic crystal.** The real part of (a) $G_{\perp}\left(z, \lambda = \frac{2\pi c}{\omega}, \theta = \sin^{-1}\left(\frac{qc}{\omega}\right) = 0\right)$ and (b) $G_{\perp}(z, \lambda, \theta = 0)$ vs. distance from the interface and emission wavelength, in the first 10 periods of a LYSO\air PhC. The dark vertical stripes correspond to the layers that do not have luminescence centers (no scintillation). The colored stripes show that the PhC features, including the photonic bandgap, are formed within a few layers from the interface. From the plot we notice that $G_{\perp}$ has a maximum in the center of each scintillation layer, while $G_{||}$ has a minimal value at the same points, for the specific band of interest. We note that for different bands, or with different refractive indices of the materials, the typical shapes of $G_{\perp}$ and $G_{||}$ can alternate.

To find the Purcell enhancement, we can use the expression in Eq. (S15), though our structure enables to further simplify the expression when investigating emission only into modes that are propagating in media $m$. In such a case, we may substitute $\hat{\boldsymbol{q}} = \cos\phi\hat{x} + \sin\phi\hat{y}$ and integrate over the in-plane angle $\phi$, in addition to a change of variables $q = k_m \sin\theta$ , $k_{m,z} = k_m \cos\theta$, so that the expression for the Green's function becomes:

$$\mathrm{Im}\overleftrightarrow{\mathbf{G}}(\boldsymbol{r},\boldsymbol{r};\omega)=k_m\int_0^{\frac{\pi}{2}}d\theta\,\frac{\sin\theta}{8\pi}\left[\begin{pmatrix}1&0&0\\0&1&0\\0&0&0\end{pmatrix}\left(\cos^2\theta\,\mathrm{Re}\{G_{\parallel}^{TM}\}+\mathrm{Re}\{G_{\parallel}^{TE}\}\right)+\begin{pmatrix}0&0&0\\0&0&0\\0&0&1\end{pmatrix}2\sin^2\theta\,\mathrm{Re}\{G_{\perp}^{TM}\}\right].$$

We note that a precise expression includes an integral over $q$ until infinity instead of $\theta$.

In order to get the enhancement for a randomly oriented dipole, we use the identity that the average over all directions equals one third of the Green's function trace. The total emission rate enhancement, denoted by the Purcell factor $F_{\mathrm{p}}$, is:

$$F_{\mathrm{p}}=\frac{1}{3}\frac{6\pi}{k_0}\left[\mathrm{Im}\left\{\mathrm{Tr}\left[\overleftrightarrow{\mathbf{G}}\left(\boldsymbol{r},\boldsymbol{r};\omega_0\right)\right]\right\}\right]=\sqrt{\varepsilon(\omega)}\int_0^{\frac{\pi}{2}}d\theta\,\sin\theta\,\frac{\cos^2\theta\,\mathrm{Re}\{G_{\parallel}^{TM}\}+\sin^2\theta\,\mathrm{Re}\{G_{\perp}^{TM}\}+\mathrm{Re}\{G_{\parallel}^{TE}\}}{2}. \quad \text{(S18)}$$

Notice that Eq. (18) is consistent with a Purcell factor of $\sqrt{\varepsilon(\omega)}$ for a bulk material (when $G_{\perp,\parallel}^{\sigma}=1$) for any homogeneous media. From Eq. (S18), the expression for the spectral and angular Purcell factor in a specific location is

$$F_P(z,\omega,\theta)=\sqrt{\varepsilon(\omega)}\,\frac{\cos^2\theta\,\mathrm{Re}\{G_{\parallel}^{TM}\}+\sin^2\theta\,\mathrm{Re}\{G_{\perp}^{TM}\}+\mathrm{Re}\{G_{\parallel}^{TE}\}}{2}. \quad \text{(S19)}$$

The expression in Eq. (S19) is exactly the factor that needs to be substituted in Eq. (S5) in order to find the enhanced scintillation parameters in Section S.2, with emission rates for each polarization $\Gamma_0^{\sigma}=\frac{\Gamma_0}{2}$, and Purcell factors of $F_P^{TM}(z,\omega,\theta)=\cos^2\theta\,\mathrm{Re}\{G_{\parallel}^{TM}\}+\sin^2\theta\,\mathrm{Re}\{G_{\perp}^{TM}\}$, and $F_P^{TE}(z,\omega,\theta)=\mathrm{Re}\{G_{\parallel}^{TE}\}$. Noticeably, a more general derivation, which we use in the main text, includes the representation of the integrals in Eqs. (S18-S19) with the in-plane momenta $\boldsymbol{q}$ instead of the emission angle (denoted as $k_x$ in Fig. 2a), since the in-plane momenta is not limited. We also note that the methodology above needs to assume slight losses for predicting the emission rate above the critical angle of the layers near the edge. In Figure S.2, we present the Purcell factor near the edge of a finite photonic crystal, when fixing each parameter in the problem.

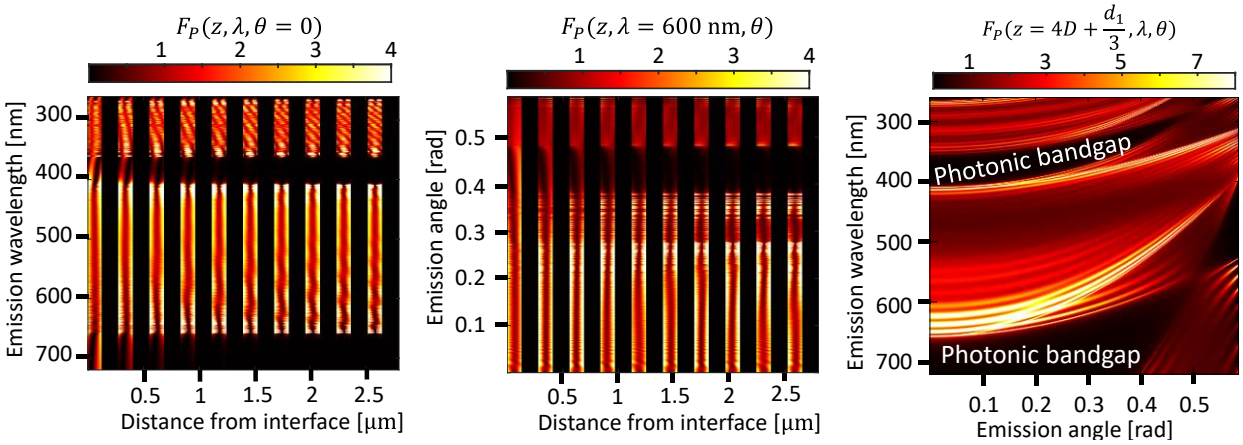


**Figure S2: The Purcell factor $F_P(z,\lambda,\theta)$, presented through cross-section plots. (a)** The Purcell factor for perpendicular emission, $F_P(z,\lambda,\theta=0)$. In this plot we see similar features as in Fig. (S1b) since only $G_\parallel$ contributes to the emission. **(b)** The Purcell factor for a specific wavelength, $F_P(z,\lambda=600\text{ nm},\theta)$. In (a) and (b) the dark vertical stripes correspond to the layers that do not have luminescence centers (no scintillation). **(c)** The Purcell factor in a specific location in space, $F_P\left(z=4D+\frac{d_1}{3},\lambda,\theta\right)$, where $D$ and $d_1$ are the period and LYSO layer length respectively. In this plot, the photonic crystal features are clearly seen, though having a finite number of periods creates a fringe-like pattern. In all plots, the luminescence centers are assumed homogeneous and with random dipole orientations.

In the main text, we present the results for a scintillator in which the dipoles of the luminescence centers are oriented in a fixed direction (Fig. 2c), showing that finding such a design would enhance the scintillation process. If the dipoles are oriented in a fixed direction inside the scintillator (denoted by the $\hat{\boldsymbol{\mu}}$ direction), the Purcell factor gets the form $F_\mathrm{p} = \frac{6\pi}{k_m}\left[\mathrm{Im}\{\overleftrightarrow{\mathbf{G}}_{\hat{\boldsymbol{\mu}}\hat{\boldsymbol{\mu}}}(\boldsymbol{r},\boldsymbol{r};\omega_0)\}\right]$. Specifically, for a dipole oriented in angle $\theta_{\hat{\boldsymbol{\mu}}}$ (relative to the z axis), the dipole orientation is $\hat{\boldsymbol{\mu}} = \sin(\theta_{\hat{\boldsymbol{\mu}}})\,\hat{\boldsymbol{x}} + \cos(\theta_{\hat{\boldsymbol{\mu}}})\,\hat{\boldsymbol{z}}$, leading to a Purcell factor:

$$F_{P,\theta_{\hat{\boldsymbol{\mu}}}}(z,\omega,\theta) = \frac{3}{4}\left[\sin^2(\theta_{\hat{\boldsymbol{\mu}}})\left(\cos^2\theta\,\mathrm{Re}\{G_\parallel^{TM}\} + \mathrm{Re}\{G_\parallel^{TE}\}\right) + 2\cos^2(\theta_{\hat{\boldsymbol{\mu}}})\sin^2\theta\,\mathrm{Re}\{G_\perp^{TM}\}\right].$$

In this case, the Purcell factors per polarizations are $F_{P,\theta_{\hat{\boldsymbol{\mu}}}}^{TM}(z,\omega,\theta) = \frac{3}{2}\sin^2(\theta_{\hat{\boldsymbol{\mu}}})\cos^2\theta\,\mathrm{Re}\{G_\parallel^{TM}\} + 3\cos^2(\theta_{\hat{\boldsymbol{\mu}}})\sin^2\theta\,\mathrm{Re}\{G_\perp^{TM}\}$, and $F_{P,\theta_{\hat{\boldsymbol{\mu}}}}^{TE}(z,\omega,\theta) = \frac{3}{2}\sin^2(\theta_{\hat{\boldsymbol{\mu}}})\,\mathrm{Re}\{G_\parallel^{TE}\}$.

## S.5 Deriving the Purcell factor for an infinite photonic crystal

In this section, we exploit the symmetry of an infinitely periodic structure to find the reflection coefficients and derive the Purcell factor. In such structure, the reflection coefficients are also periodic, leading to $\tilde{R}^{\sigma}_{m,m+1} = \tilde{R}^{\sigma}_{m,m-1} = \tilde{R}^{\sigma}_{m+2,m+3}$. By looking at specific layers $m = 1,2$ with width $d_{1,2}$, we find

$$\tilde{R}_{1,2} = \frac{r_{1,2} + \tilde{R}_{2,1} e^{2ik_{2,z}d_2}}{1 + r_{1,2}\tilde{R}_{2,1} e^{2ik_{2,z}d_2}}, \qquad \tilde{R}_{2,3} = \tilde{R}_{2,1} = \frac{r_{2,1} + \tilde{R}_{1,2} e^{2ik_{1,z}d_1}}{1 + r_{2,1}\tilde{R}_{1,2} e^{2ik_{1,z}d_1}},$$

leading to a quadratic equation for $\tilde{R}_{1,2}$:

$$\tilde{R}^2_{1,2} r_{12} e^{2ik_{1,z}w_1}\left(e^{2ik_{2,z}d_2} - 1\right) + \tilde{R}_{1,2}\left(1 - r_{12}^2\left(e^{2ik_{2,z}d_2} + e^{2ik_{1,z}d_1}\right) - e^{2i\left(k_{1,z}d_1 + k_{2,z}d_2\right)}\right) + r_{12}\left(e^{2ik_{2,z}d_2} - 1\right) = 0.$$

Although the equation results in two possible solutions, we choose only the single solution which satisfies $\left|\tilde{R}_{1,2}\right|^2 \leq 1$. After finding $\tilde{R}^{\sigma}_{1,2}(\omega, q)$ for each polarization, wavevector**,** and frequency, we can substitute it back in the expression for $G^{\sigma}_{\perp,\parallel}$ in Eq. (S16). So that for the $m^{\text{th}}$ layer these functions reduce to:

$$G^{\sigma}_{\parallel}(z, q, \omega) = \frac{1 + 2\tilde{R}^{\sigma}_{m,m+1} e^{ik_{m,z}d_m} \cos\left(2k_{m,z}z\right) + \left(\tilde{R}^{\sigma}_{m,m+1} e^{ik_{m,z}d_m}\right)^2}{1 - \left(\tilde{R}^{\sigma}_{m,m+1} e^{ik_{m,z}d_m}\right)^2}, \tag{S20a}$$

$$G^{TM}_{\perp}(z, q, \omega) = \frac{1 - 2\tilde{R}^{\sigma}_{m,m+1} e^{ik_{m,z}d_m} \cos\left(2k_{m,z}z\right) + \left(\tilde{R}^{\sigma}_{m,m+1} e^{ik_{m,z}d_m}\right)^2}{1 - \left(\tilde{R}^{\sigma}_{m,m+1} e^{ik_{m,z}d_m}\right)^2}, \tag{S20b}$$

which are plotted in Fig. S3. Notice that the only dependence on $z$ is through $\tilde{R}^{\sigma}_{m,m+1} \cos\left(2k_{1,z}z\right)$, enabling to calculate the average of the Purcell factor over space analytically.

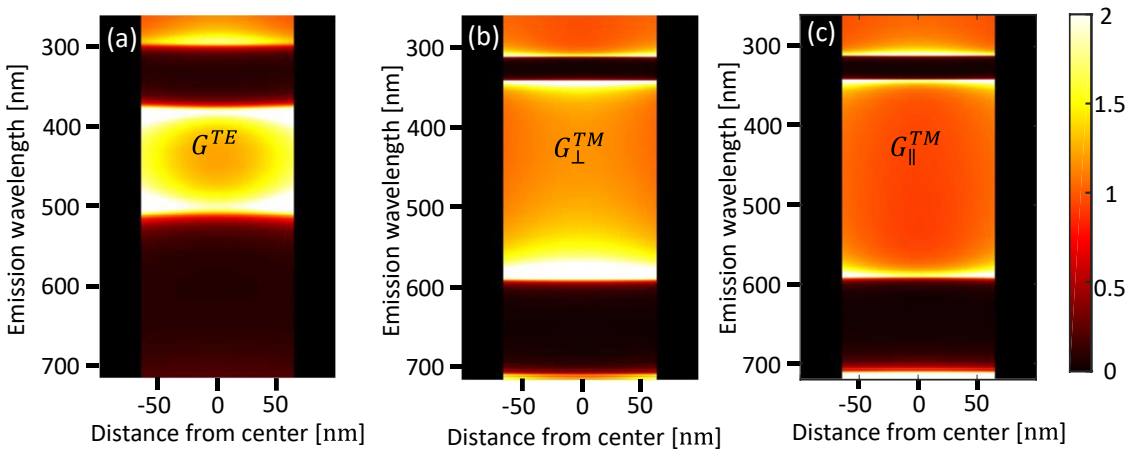


**Figure S3: The typical spectral response for an infinite Photonic crystal.** The real part of **(a)** $G^{TE}\left(z,\lambda,\theta=\frac{\pi}{8}\right)$, **(b)** $G_{\perp}^{TM}\left(z,\lambda,\theta=\frac{\pi}{8}\right)$ and **(c)** $G_{\parallel}^{TM}\left(z,\lambda,\theta=\frac{\pi}{8}\right)$ vs. the distance from the center of the LYSO layer and the emission wavelength, in a LYSO\air PhC. We see that $G_{\perp}$ has a maximum in the center of the LYSO layer, while $G_{||}$ has a minimum in that point, for the main photonic band of interest (as oppose to the higher band that has an opposite behavior). Since the angle of emission is not zero, the energies of the photonic bandgap are polarization-dependent (TE or TM).

## S.6 The photonic structure's partial emission properties

In the previous sections, we derived both the integrated expressions such as $\eta$ and $\Gamma_{\text{eff}}$ that describe the structure as a whole, and the local expressions such as $F_P^\sigma(z,\omega,\theta)$. In this section, we derive expressions that focus on specific emission properties, as the angular or spectral emission. With these expressions, our optimization approach can be used to maximize different emission figure-of-merits according to the required application. The Purcell factor $F_P^\sigma$ is normalized to the emission rate in vacuum. However, it is valuable to also define the emission rate enhancement relative to the bulk emission rate $F_{P,\mathrm{b}}^\sigma$, and the emission rate enhancement into detectable photons, relative to the equivalent in a bulk, $F_{P,\mathrm{det}}^\sigma$.

We define the Purcell factor averaged over space in the following way:

$$F_P^\sigma(\omega,\theta)=\int \mathrm{d}z G(z) P_F^\sigma(\mathrm{z},\omega,\theta),\quad F_{P,\mathrm{b}}^\sigma(\omega,\theta)=\frac{\int \mathrm{d}z G(z) F_P^\sigma(\mathrm{z},\omega,\theta)}{\sqrt{\varepsilon(\omega)}},$$

$$F_{P,\mathrm{det}}^\sigma(\omega,\theta)=\frac{\int \mathrm{d}z G(z) F_P^\sigma(\mathrm{z},\omega,\theta)\, T^\sigma(\mathrm{z},\omega,\theta)}{\sqrt{\varepsilon(\omega)} T_0^\sigma(\omega,\theta)}. \qquad \text{(S21a, b, c)}$$

We note that Eq. (S21b) is plotted in Fig. 2a in the main text for each of the two polarizations. By integrating Eqs. (S21) over frequency (weighted by the spectrum of the scintillator's luminescence centers), we find the angular Purcell factors

$$P_F^\sigma(\theta)=\int \mathrm{d}\omega \int \mathrm{d}z G(z) Y(\omega) F_P^\sigma(\mathrm{z},\omega,\theta),\qquad F_{P,\mathrm{b}}^\sigma(\theta)=\frac{\int \mathrm{d}\omega \int \mathrm{d}z G(z) Y(\omega) F_P^\sigma(\mathrm{z},\omega,\theta)}{\int \mathrm{d}\omega Y(\omega)\sqrt{\varepsilon(\omega)}},$$

$$F_{P,\mathrm{det}}^\sigma(\theta)=\frac{\int \mathrm{d}\omega Y(\omega) \int \mathrm{d}z G(z) F_P^\sigma(\mathrm{z},\omega,\theta)\, T^\sigma(\mathrm{z},\omega,\theta)}{\int \mathrm{d}\omega Y(\omega) T_0^\sigma(\omega,\theta)\sqrt{\varepsilon(\omega)}}. \qquad \text{(S22a, b, c)}$$

The plot of Eq. (S22b) can be found in the turquoise plot in Fig. 2b, while the blue plot in the same figure is derived from $\frac{\int \mathrm{d}\omega \int \mathrm{d}z G(z) Y(\omega) F_P^\sigma(\mathrm{z},\omega,\theta) T^\sigma(\mathrm{z},\omega,\theta)}{\int \mathrm{d}\omega Y(\omega)\sqrt{\varepsilon(\omega)}}$ so that the ratio between the two plot areas

presents the percentage of the emitted light that can couple out of the structure. In Fig. S4, we present similar quantities for structures that were optimized for emission at a particular angle, specifically maximizing $P^{\sigma}_{F,\mathrm{b}}(\theta=0)$ (blue), and $\frac{F^{\sigma}_{P,\mathrm{det}}(\theta=\pi/3)}{F^{\sigma}_{P,\mathrm{det}}(\theta=0)}$ (pink). In the expression for the pink simulation, the emission directionality is separated from the efficiency. This separation provides an example of the role of each part in the total enhancement that was the focus of the paper, both the enhancement of the emission rate and the focusing of the angular spread.

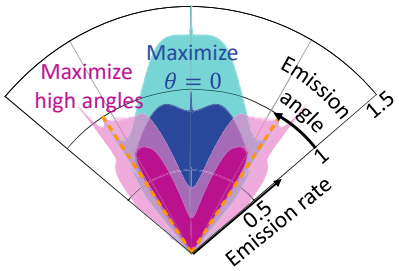


**Figure S4: Control over the emission direction.** The total emission rate from the PhC (turquoise and light pink) and the outcoupled part (blue and deep pink), normalized by the bulk emission rate. The blue (pink) plot describes an emission of the structure that maximizes the zero-angle (high angle) emission rate. The ratio between the blue and turquoise (and deep to light pink) plots show that the overall efficiency of these structures is smaller compared to Fig. 2b because they were optimized for specific angles instead of the total emission. This way we get that the deep pink plot presents a highly directional emission, but with a small effective emission rate.

Finally, using a weighted angular integral over Eqs. (S21), we reach the Purcell factors as a function of frequency

$$F^{\sigma}_{P}(\omega)=\int_{0}^{\frac{\pi}{2}}\sin(\theta)\,\mathrm{d}\theta\int \mathrm{d}z G(z)F^{\sigma}_{P}(\mathrm{z},\omega,\theta)\;;\;F^{\sigma}_{P,\mathrm{b}}(\omega)=\frac{1}{\sqrt{\varepsilon(\omega)}}\int_{0}^{\frac{\pi}{2}}\sin(\theta)\,\mathrm{d}\theta\int \mathrm{d}z G(z)F^{\sigma}_{P}(\mathrm{z},\omega,\theta)$$

$$F^{\sigma}_{P,\mathrm{det}}(\omega)=\frac{\int_{0}^{\frac{\pi}{2}}\sin(\theta)\,\mathrm{d}\theta\int \mathrm{d}z G(z)F^{\sigma}_{P}(\mathrm{z},\omega,\theta)\,T^{\sigma}(\mathrm{z},\theta,\omega)}{\int_{0}^{\frac{\pi}{2}}\sin(\theta)\,\mathrm{d}\theta\,T^{\sigma}_{0}(\theta,\omega)\sqrt{\varepsilon(\omega)}}. \qquad \text{(S23a, b)}$$

Overall, we presented in this section several possible expressions that can be used as a figure-of-merit for optimizing the photonic structure.

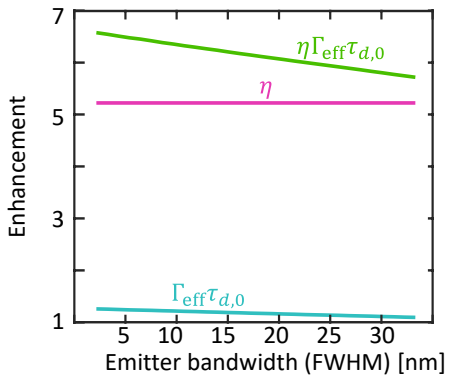


**Figure S5:** The control over the efficiency $\eta$ and effective emission rate $\Gamma_{\mathrm{eff}}$ by manipulating the spectral bandwidth of the emitters. The emitter spectral distribution $Y(\omega)$ was modeled as a gaussian in frequency. The other parameters in the problem, such as each the layers' widths, remained the same as the optimized LYSO\air PhC with the original spectral distribution (similar to Fig. 2). Unsurprisingly, the results show an improvement in all optimization parameters when reducing the bandwidth, but since the quality factor of the optical structure is small, this improvement is accordingly not significant.

**Table S1: Simulation parameters.** The table concentrates the parameters used in each plot in the manuscript and SM. The refractive indices of the scintillator layers, the other dielectric layers, and the surrounding material, are denoted by $n_1$,$n_2$, and $n_{\text{ext}}$ respectively. $d_{1,2}$ denote the width of the scintillator layer and of the dielectric layer respectively. In each figure that include an optimization simulation, we denote the figure-of-merit that was used to determine $d_1$ and $d_2$.

| Plot | $n_1$ | $n_2$ | $n_{\text{ext}}$ | optimization parameter | $d_1$ [nm] | $d_2$ [nm] |
|---|---|---|---|---|---|---|
| Fig. 1– blue curves<br>Figs. 2, S1, S2, S3 | 1.81 | 1 | 1 | $\eta\Gamma_{\text{eff}}$ | 130 | 150 |
| Fig. 1a – red curves | 2.3 | 1.5 | 1.5 | $\eta\Gamma_{\text{eff}}$ | 130 | 130 |
| Fig. 3a<br>Fig. S5 | 1.81 | 1 | 1 | - | 130 | 150 |
| Fig. S4 – blue curves | 1.81 | 1 | 1 | $P_F(\theta = 0)$ | 85 | 41 |
| Fig. S4 – pink curves | 1.81 | 1 | 1 | $\frac{P^{\sigma}_{F,\text{det}}(\theta = \pi/3)}{P^{\sigma}_{F,\text{det}}(\theta = 0)}$ | 41 | 85 |
| Fig. 3b | 1.81 | 1 | 1 | - | 130± rand(x) | 150 |

## References

[1] R. F. Post and L. I. Schiff, Phys. Rev. **80**, 1113 (1950).

[2] L. Novotny and B. Hecht, *Principles of Nano-Optics* (Cambridge University Press, Cambridge, 2012).

[3] W. C. Chew, *Waves and Fields in Inhomogenous Media* (IEEE, 1999).

[4] J. A. E. Wasey and W. L. Barnes, J. Mod. Opt. **47**, 725 (2000).